3D Plotted PCL Scaffolds for Stem Cell Based Bone Tissue Engineering

Pinar Yilgor,[1,2] *Rui A. Sousa,*[3,4] *Rui L. Reis,*[3,4] *Nesrin Hasirci,*[2,5] *Vasif Hasirci**[1,5]

Summary: The ability to control the architecture and strength of a bone tissue engineering scaffold is critical to achieve a harmony between the scaffold and the host tissue. Rapid prototyping (RP) technique is applied to tissue engineering to satisfy this need and to create a scaffold directly from the scanned and digitized image of the defect site. Design and construction of complex structures with different shapes and sizes, at micro and macro scale, with fully interconnected pore structure and appropriate mechanical properties are possible by using RP techniques. In this study, RP was used for the production of poly(ε-caprolactone) (PCL) scaffolds. Scaffolds with four different architectures were produced by using different configurations of the fibers (basic, basic-offset, crossed and crossed-offset) within the architecture of the scaffold. The structure of the prepared scaffolds were examined by scanning electron microscopy (SEM), porosity and its distribution were analyzed by micro-computed tomography (μ-CT), stiffness and modulus values were determined by dynamic mechanical analysis (DMA). It was observed that the scaffolds had very ordered structures with mean porosities about 60%, and having storage modulus values about 1×10^7 Pa. These structures were then seeded with rat bone marrow origin mesenchymal stem cells (MSCs) in order to investigate the effect of scaffold structure on the cell behavior; the proliferation and differentiation of the cells on the scaffolds were studied. It was observed that cell proliferation was higher on offset scaffolds (262000 vs 235000 for basic, 287000 vs 222000 for crossed structure) and stainings for actin filaments of the cells reveal successful attachment and spreading at the surfaces of the fibers. Alkaline phosphatase (ALP) activity results were higher for the samples with lower cell proliferation, as expected. Highest MSC differentiation was observed for crossed scaffolds indicating the influence of scaffold structure on cellular activities.

Keywords: mesenchymal stem cell; poly(ε-caprolactone); rapid prototyping; scaffold; tissue engineering

Introduction

Bone tissue has the capacity of self-reconstruction upon injury, however, when the defect is large it usually remains unrepaired[1] and require a filler, such as cadaver bone, coral, hydroxyapatite or similar mineral compounds. A tissue engineered scaffold with tailored structural and mechanical properties would be an ideal filler. Conventional tissue engineering scaffold production techniques such as fiber bonding,[2] solvent casting/particulate leaching,[3] membrane lamination,[4] melt

[1] METU, BIOMAT, Department of Biological Sciences, Biotechnology Research Unit, 06531 Ankara, Turkey
Fax: 90.312.2101542;
E-mail: vhasirci@metu.edu.tr
[2] METU, BIOMAT, Department of Chemistry, 06531 Ankara, Turkey
[3] 3B's Research Group- Biomaterials, Biodegradables and Biomimetics, University Minho, 4710-057 Braga, Portugal
[4] IBB - Institute for Biotechnology and Bioengineering, PT Associated Laboratory, Braga, Portugal
[5] METU, BIOMAT, Department of Biomedical Engineering, 06531 Ankara, Turkey

molding[5] and gas foaming,[6] generally lack the ability to produce structures with predefined homogeneous structure. Instead, they have such drawbacks as poor reproducibility, irregularity of pore shape and insufficient pore interconnectivity.

3D geometry of tissue engineering scaffolds is very important as it has a profound effect on cell behavior in a successful tissue engineered construct. In the study of Kenar *et al.* effect of alignment on MSC proliferation and differentiation was investigated on micropatterned poly(3-hydroxybutyrate-co-3-hydroxyvalerate) (PHBV) and poly(L/D,L-lactic acid) (P(L/DL)A) blend films.[7] It was observed that alignment positively influenced the differentiation of MSCs into osteoblasts. In a similar study, the effect of contact guidance on the construction of a corneal stroma was investigated on keratocyte seeded collagen films.[8] It was reported that patterning induced the oriented secretion of the extracellular matrix therefore improving the properties of the construct.

It is known that the maintenance of cellular activities and interconversions of the connective-tissue cells (fibroblasts, cartilage cells and bone cells) are highly dependent on their shape and anchorage which controls their gene expression.[9] The arrangement within the architecture of a scaffold defines the geometry of the adhesion sites for the cells, thus determine their adhesion, degree of spreading and cytoskeleton orientation. Therefore, it was stated that the cellular mobility, proliferation and differentiation is dictated by the initial attachment geometry and the strength of it. The control of cellular activities is especially important in the case of stem cell based tissue engineering therapies in which controlled proliferation and differentiation of stem cells is of utmost importance.

Rapid prototyping (RP) technique is attracting more and more attention because it is the ideal tool for creating a scaffold directly from the scanned image and the computer model of the defect site to provide a structurally and mechanically perfect fit.[10] It is the process of creating 3D objects through repetitive deposition of material layers, a typical bottom-up approach, using computer-controlled equipment, based on the cross-sectional data obtained from slicing a computer-aided design (CAD) model of the object.[11] Besides having precise control over porosity, pore size, stiffness and permeability; the RP scaffolds are usually designed to have a fully interconnected pore structure.[12] While creating scaffolds with defined structure and architecture, RP techniques also allow the investigation of the effect of scaffold geometry on cell behavior for further optimization of the scaffold design.

Recent developments in solid free-form fabrication techniques and improvement of systems which can utilize polymers have made it possible to design and manufacture tailor-made tissue engineering scaffolds with precise control. There are several approaches for the production of RP scaffolds such as selective laser sintering (SLS),[13] fused deposition modeling (FDM),[14] 3D fiber deposition[15] or 3D plotting.[16] Among the available fabrication techniques, 3D plotting is the most convenient method due to its milder operation conditions, absence of left over polymer powder within the scaffold and the ability to produce scaffolds without any binders. Thus, 3D plotting appeared to be a very appropriate method for producing bone tissue engineering scaffolds.

Poly(ε-caprolactone) (PCL) is a fully biodegradable, thermoplastic polyester with potential applications for bone and cartilage repair and was successfully used as a scaffold material in various forms.[17–18] PCL has thermal stability in molten state due to its such favorable properties as low glass transition temperature ($-60\,^{\circ}C$), low melting temperature ($60\,^{\circ}C$) and high decomposition temperature ($350\,^{\circ}C$).[19] PCL degrades very slowly, much slower than PLGA or PHBV, due to its high hydrophobicity and crystallinity[20] therefore it is suitable for use in long term load bearing applications. A number of studies are being carried out using PCL biocomposites and copolymers with both natural and synthetic polymers.[19,21] PCL scaffolds

have been created with a variety of RP techniques including FDM[22], shape deposition modeling[23], SLS[24], low-temperature deposition[25] and multi-nozzle free-form deposition.[26-27] It was observed in these systems that the cells adhere and start growing on the PCL scaffolds and the applicability of the produced scaffolds were demonstrated *in vitro* and *in vivo*. However, the fabrication and characterization of PCL scaffolds with varying architectures made through 3D plotting has not been reported.

In this study, 3D plotting was used for the production of poly(ε-caprolactone) (PCL) scaffolds for bone tissue engineering purpose. SEM, μ-CT and DMA analyses were performed to characterize the produced structures in terms of structure, porosity and mechanical properties. Scaffolds were produced with four different architectures by changing the configuration of the deposited fibers within the architecture. This study intends to investigate the effect of scaffold structure on the structural and mechanical properties as well as the effects on stem cell behavior.

Materials and Methods

Materials

Poly(ε-caprolactone) (MW = 37000) was purchased from Solvay Caprolactones under the trade name CAPA 6404 (UK). Dulbecco's Modified Eagle Medium (DMEM; high glucose) was supplied by Gibco (USA). Fetal calf serum, trypsin/EDTA, penicillin/streptomycin, Amphothericin B, glutaraldehyde, formaldehyde, cacodylic acid (sodium salt), dexamethasone, β-glycerophosphate disodium salt, L-ascorbic acid were bought from Sigma-Aldrich (Germany). NucleoCounter reagents were supplied by Chemometec (Denmark) and Alamar Blue cell proliferation assay solution was from USBiological. For the assessment of cell differentiation, alkaline phosphatase kit (Randox, USA) was used.

Scaffold Fabrication

Scaffolds were fabricated with a Bioplotter® (Envisiontec GmbH, Germany). Briefly, PCL was placed in a stainless steel syringe and processed at 130 °C through a heated cartridge unit. When the polymer melted, a CO_2 pressure was applied to the syringe through a pressurized cap. Rectangular block models (20 × 20 mm of projected area) were loaded on the Bioplotter CAD/CAM software and scaffold was plotted layer-by-layer, through the extrusion of the polymer as a fiber, up to 10 layers. Scaffolds with different architectures were produced by changing the respective orientation of the deposited fibers. PCL scaffolds were produced according to four different standard architectures, namely: basic (B), basic-offset (BO), crossed (C) and crossed-offset (CO) structures. The B architecture is produced by the consecutive deposition of 2D layers, in which layer N is plotted orthogonally to layer N-1, and is plotted in the same relative position of layer N-2. The BO architecture is similar to B, but layer N is plotted with in an offset distance relative to layer N-2. The C architecture is produced by the consecutive deposition of 2D layers, in which layer N is plotted diagonally to layer N-1, and is plotted in the same relative position of layer N-4. The CO architecture is similar to C, but layer N is plotted with in an offset distance relative to layer N-4. Final scaffolds were obtained using a circular cutting die with 5 mm of diameter.

Scaffold Characterization

Structure and geometry of the scaffolds were investigated by using a scanning electron microscope (Leica Cambridge S360, Germany) after sputter coating with gold.

Porosity and porosity distribution were assessed by using micro-computed tomography (μ-CT 20, SCANCO Medicals, Switzerland). Scanner settings were 40 keV and 248 μA. Entire scaffolds were scanned in around 200 slices each of 7 μm thickness. 3 samples were analyzed for each scaffold architecture. CT Analyser and CT Vol Realistic 3D Visualization (SkyScan, Belgium) softwares were used for image processing in CT reconstructions, and to create and visualize the 3D representations.

Dynamic mechanical analysis (Perkin Elmer DMA7e, USA) was used as a tool to

relate material behavior with the molecular structure, processing conditions and product properties. An oscillating compressive force was applied to the dry sample at 37 °C and the resulting displacement of the sample was measured, and from this, the stiffness of the sample and the sample modulus were calculated. The real (storage) modulus, E', and the imaginary (loss) modulus, E'', components of the complex modulus, E^* (where $E^* = E' + iE''$), were recorded against frequency that varied between 0.1 and 70 Hz.

Cell Culture

Bone marrow mesenchymal stem cells were isolated from 6 week old, male Sprague Dawley rats. The rats were euthanized and their femurs and tibia were excised, washed with DMEM containing 1000 U/mL penicillin and 1000 μg/mL streptomycin under aseptic conditions. The marrow residing in the midshaft was flushed out with DMEM containing 20% fetal calf serum (FCS) and 100 U/mL penicillin and 100 μg/mL streptomycin, the cells were centrifuged at 500 g for 5 min, the resulting cell pellet was resuspended and plated in T-75 flasks. These primary cultures were incubated for 2 days. The hematopoietic and other unattached cells were removed from the flasks by repeated washes with phosphate buffer saline (PBS) (10 mM, pH 7.4) and the medium of the flasks was renewed every other day until confluency is reached. These primary cultures were then stored frozen in liquid nitrogen until use. Seeding density on the scaffolds was 50000 cells per scaffold. Incubation was performed at 37 °C and 5% CO_2 in DMEM supplemented with 10% FCS, 10 mM β-glycerophosphate, 50 μg/mL L-ascorbic acid, 10 nM dexamethasone and penicillin/streptomycin/amphotericin B. Viable cell number was assessed with Alamar Blue assay (USBiological). ALP activity was determined by using Randox kit (USA). The absorbance of p-nitrophenol formed from p-nitrophenyl phosphate was determined at 405 nm and calculation of enzyme amount was as described by the manufacturer. Cell seeded scaffolds were fixed with 4% p-formaldehyde in PBS (pH 7.4) for 15 min at the end of 21 days of incubation, and treated with triton X-100 (1%) for 5 min to permeabilize the cell membranes. Samples were then incubated at 37 °C for 1 h in bovine serum albumin (BSA)-PBS (1%) solution prior to staining with FITC-labeled phalloidin (for actin filaments). The samples were studied with a confocal microscope (Leica TCS SPE, Germany).

Results and Discussion

Scaffold Production and Characterization

PCL scaffolds were prepared with four different standard architectures designated as basic (B), basic-offset (BO), crossed (C) and crossed-offset (CO) structures (Figure 1).

Scaffold Porosity

The porosity and porosity distribution of the scaffolds were investigated by using μ-CT. The porosity (%) values of the scaffolds indicate that the porosity of the scaffolds are in the range 50–70% and are somewhat dependent on the fiber orientation within the construct (Table 1). It was also observed that the pores were completely interconnected throughout the whole structure. The porosity profiles showed that the porosity from top to bottom of the scaffolds did not have a significant change as expected from the precision of the production method of the scaffolds by exact placement of the polymer fibers during the layer-by-layer deposition by the Bioplotter (Figure 2). This is especially important when most scaffolds produced by other methods do not have complete connectivity and the porosity decreases as one goes from the surface towards the core leading to insufficient population and oxygen/nutrient concentrations in the core.

Mechanical Properties

The stiffness, the storage and loss modulus values of the samples were calculated by DMA analysis (Table 2). It was observed that the change in fiber orientation in the

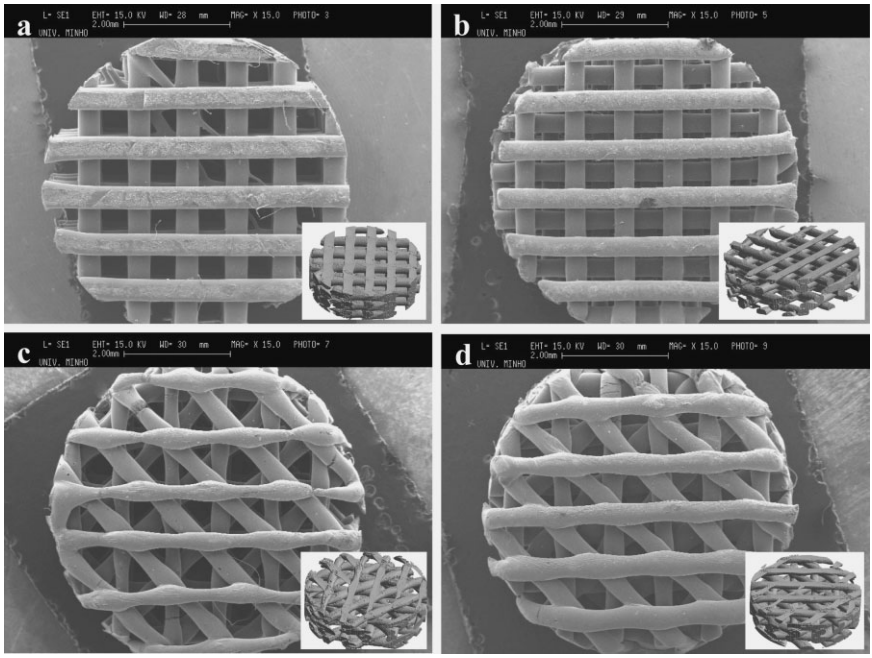

Figure 1.
SEM images of PCL scaffolds produced by the Bioplotter with different architectures. (a) B, (b) BO, (c) C, (d) CO (×15). Inset pictures are the μ-CT images of these scaffolds.

scaffold from BO to B architecture results in an increase in storage modulus from $3.48 \pm 0.08 \times 10^6$ Pa to $1.85 \pm 0.19 \times 10^7$ Pa; while loss modulus increased from $2.64 \pm 0.07 \times 10^5$ Pa to $8.80 \pm 0.01 \times 10^5$ Pa. Therefore, it can be stated that the mechanical properties of a 3D plotted scaffold can be, to some extend, tuned through the adjustment of the fiber positioning within the scaffold architecture, allowing for its adaptation different tissue mechanical requirements.

The storage moduli for cortical, demineralized cortical and trabecular bone were reported to be 8×10^9, 2×10^9 and 8×10^5 Pa, respectively. The loss moduli for the same samples were 2×10^8, 7.5×10^7 and 5.2×10^4 Pa, respectively.[28-29] Therefore, the PCL scaffolds exhibit higher stiffness as compared to trabecular and lower stiffness relatively to cortical bone in terms strorage and loss moduli. Nevertheless, in order to resist to the mechanical stresses in a cortical bone implantation, these scaffolds should be stiffer. However, it should be kept in mind that the stiffness and strength in bone are the result of the nano-scaled organization of mineral and organic fractions. Since the scaffolds cannot replicate such high mechanical performance, it is expected that the construct upon cell proliferation and ECM secretion achieves comparable mechanical properties to a living bone.

Table 1.
Mean porosity values of the scaffolds.

Scaffold	Mean Porosity (%)
B	50.98 ± 3.16
BO	66.31 ± 4.35
C	65.00 ± 6.01
CO	56.80 ± 6.78

This analysis also showed that the PCL scaffolds exhibit a viscoelastic behavior and that although influential, the porosity is not the sole determinant of the stiffness as other factors such as number of junction points between fibers and their relative orientation can also influence mechanical

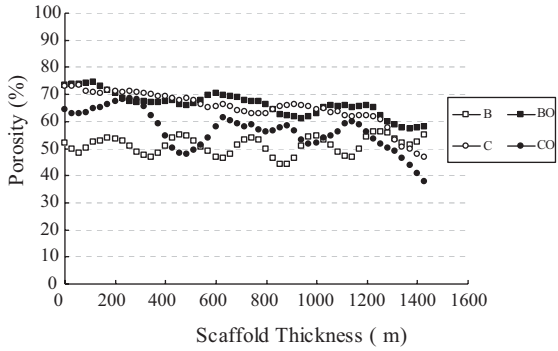

Figure 2.
Porosity distribution throughout PCL scaffolds.

properties. For example, structures BO and C demonstrated almost similar porosities (about 65%), but storage modulus values were differed about 3.3 times (from 3.48×10^6 to 1.15×10^7 Pa). When the structures are compared, it was observed that scaffolds without offset had higher compressive stiffness due to juxtaposition of consecutive filaments along the Z axis (Figure 3).

In Vitro Studies

PCL scaffolds were seeded with rat bone marrow MSCs at a density of 5×10^5 cells/scaffold to assess suitability for use in bone tissue engineering applications, proliferation and ALP activity were tested after 7, 14 and 21 days of incubation.

Table 2.
Storage and loss modulus of 3D printed PCL scaffolds.

	Storage Modulus (Pa)	Loss Modulus (Pa)
B	$1.85 \pm 0.19 \times 10^7$	$8.80 \pm 0.01 \times 10^5$
BO	$3.48 \pm 0.08 \times 10^6$	$2.64 \pm 0.07 \times 10^5$
C	$1.15 \pm 0.09 \times 10^7$	$6.12 \pm 0.05 \times 10^5$
CO	$9.69 \pm 0.14 \times 10^6$	$5.32 \pm 0.07 \times 10^5$

Cell proliferation tests demonstrated that both scaffolds with the offset resulted in significantly higher cell proliferation (Figures 4 and 5). This might be related to the higher available fiber surface area on the direct flow path of the media. During cell seeding, the relative positioning of the fibers will determine the type of flow path of the media and, to a certain extend, the cell seeding efficiency. When there is no offset, cells have a clear open path which increases the likelihood of cells passing the scaffold, unless they move laterally during seeding. On the contrary, when there is an offset structure, fibers act as obstacles to the flow providing a higher surface for cells to attach to. This leads to improved initial adhesion and subsequent higher cell numbers. For almost all scaffolds (except C), cell numbers

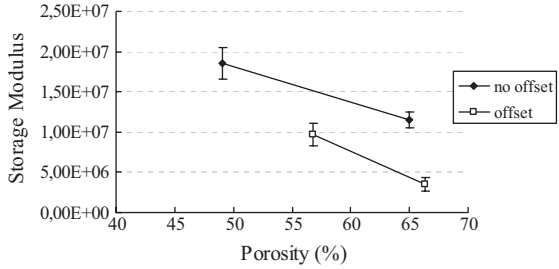

Figure 3.
Storage modulus vs. porosity for 3D printed PCL scaffolds.

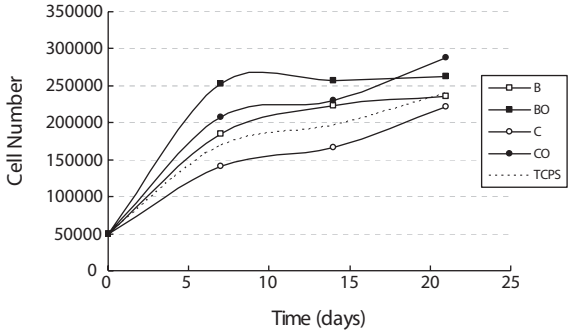

Figure 4.
MSC proliferation on PCL scaffolds.

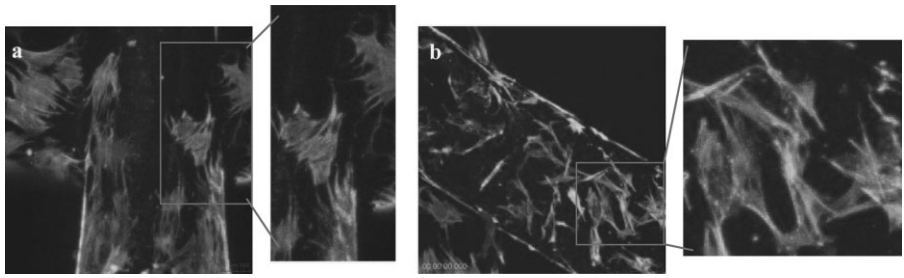

Figure 5.
FITC-labeled phalloidin staining on (a) B scaffold (x10), (b) C scaffold (×10) on day 21.

were higher than that of tissue culture polystyrene (TCPS) for all time points, which was used as a reference, indicating the successful cell-material interactions. Also, the basic (B) system had higher cell numbers which is interesting because C appears to have more (30%) porosity.

In order to determine the cell behavior and to qualitatively monitor cell growth, cell seeded scaffolds were fixed and their actin filaments were stained on day 21 (Figure 5). It was observed that the cells attach and proliferate well on the fiber surfaces of the scaffolds.

ALP activity per cell at specific time points during incubation was measured in order to investigate the degree of differentiation of MSCs into osteoblastic cells (Figure 6). As expected, there was no ALP activity during the first week. In general,

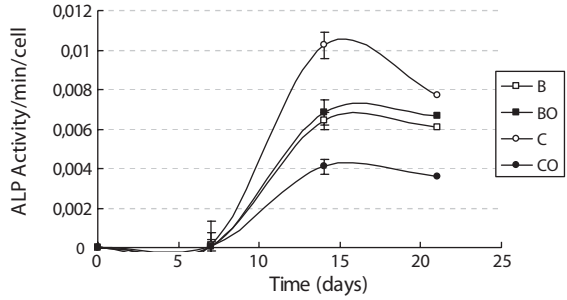

Figure 6.
Specific ALP Activity on PCL scaffolds.

ALP results are in agreement with the cell proliferation results; higher ALP activity values were obtained for samples with lower cell proliferation. Highest ALP activity was measured on the 14th day for all samples where cell proliferation rates were lowest. Highest MSC differentiation (highest ALP activity) was observed for crossed scaffold (C) in agreement with the higher proliferations with the basic types. These results indicate that scaffold architecture determines cell response, in terms of both seeding efficiency and proliferation. Furthermore, cell differentiation, as measured by ALP activity, appears to be also affected by scaffold structure, which indicates that scaffold geometry can be optimized for differentiation of MSC into the osteoblast lineage.

Conclusion

One of the most critical aspects of a scaffold intended for use as a bone substitute is the ability to structurally fit to the defect site and compensate for the inherent mechanical stresses of the site. Application of rapid prototyping techniques to the production of bone tissue engineering scaffolds is the only method available that can create such predetermined form and structures. It was shown in this study that the architecture of a scaffold determines not only the physical and mechanical properties, but also influences the cellular activities of the mesenchymal stem cells.

Acknowledgements: This project was conducted within the scope of the EU FP6 NoE Project Expertissues (NMP3-CT-2004-500283). We acknowledge the support to PY through the same project in the form of an integrated PhD grant.

[1] Carano, R. A. D. Filvaroff, E. H. *DDT* **2003**, *8*, 980–989.
[2] Tuzlakoglu, K. Bolgen, N. Salgado, A. J. Gomes, M. E. Piskin, E. Reis, R. L. *J. Mater. Sci. - Mater. Med.* **2005**, *16*, 1099–1104.
[3] Kose, G. T. Kenar, H. Hasirci, N. Hasirci, V. *Biomaterials* **2003**, *24*, 1949–1958.
[4] Mikos, A. G. Sarakinos, G. Leite, S. M. Vacanti, J. P. Langer, R. *Biomaterials* **1993**, *14*, 323–330.
[5] Se, H. O. Soung, G. K. Jin, H. L. *J. Mater. Sci. - Mater. Med.* **2006**, *17*, 131–137.
[6] Almirall, A. Larrecq, G. Delgado, J. A. Martínez, S. Planell, J. A. Ginebra, M. P. *Biomaterials* **2004**, *25*, 3671–3680.
[7] Kenar, H. Kose, G. T. Hasirci, V. *Biomaterals* **2006**, *27*, 885–895.
[8] Vrana, E. Builles, N. Hindie, M. Damour, O. Aydinli, A. Hasirci, V. *J. Biomed. Mater. Res. Part A* **2007**, *84A*, 454–463.
[9] Benya, P. D. Schaffer, J. D. *Cell* **1982**, *30*, 215–224.
[10] Yeong, W. Y. Chua, C. K. Leong, K. F. Chandrasekaran, M. *Trends Biotechnol.* **2004**, *22*, 643–652.
[11] Lam, C. X. F. Mo, X. M. Teoh, S. H. Hutmacher, D. W. *Mater. Sci. Eng. C* **2002**, *20*, 49–56.
[12] Moroni, L. de Wijn, J. R. van Blitterswijk, C. A. *Biomaterials* **2006**, *27*, 974–985.
[13] Wiria, F. E. Leong, K. F. Chua, C. K. Liu, Y. *Acta Biomater.* **2007**, *3*, 1–12.
[14] Chen, Z. Li, D. Lu, B. Tang, Y. Sun, M. Xu, S. *Scr. Mater.* **2005**, *52*, 157–161.
[15] Moroni, L. Curti, M. Welti, M. Korom, S. Weder, W. De Wijn, J. R. Van Blitterswijk, C. A. *Tissue Eng.* **2007**, *13*, 2483–2493.
[16] Oliveira, A. L. Malafaya, P. B. Costa, S. A. Sousa, R. A. Reis, R. L. *J. Mater. Sci. - Mater. Med.* **2007**, *18*, 211–223.
[17] Rai, B. Teoh, S. H. Hutmacher, D. W. Cao, T. Ho, K. H. *Biomaterials* **2005**, *26*, 3739–3748.
[18] Li, W. J. Tuli, R. Okafor, C. Derfoul, A. Danielson, K. G. Hall, D. J. Tuan, R. S. *Biomaterials* **2005**, *26*, 599–609.
[19] Hoque, M. E. Hutmacher, D. W. Feng, W. Li, S. Huang, M. H. Vert, M. Wong, Y. S. *J. Biomater. Sci. Polymer Edn* **2005**, *16*, 1595–1610.
[20] Pitt, C. G. in: *Biodegradable Polymers as Drug Delivery Systems*, M. Chasin, R. Langer, Eds., Marcel Dekker, New York, NY **1990**, P. 71.
[21] Santos, M. I. Fuchs, S. Gomes, M. E. Unger, R. E. Reis, R. L. Kirkpatrick, C. J. *Biomaterials* **2007**, *28*, 240–248.
[22] Rohner, D. Hutmacher, D. W. Cheng, T. K. Oberholzer, M. Hammer, B. *J. Biomed. Mater. Res. Part B: Appl. Biomater.* **2003**, *66B*, 574–580.
[23] Marra, K. G. Szem, J. W. Kumta, P. N. DiMilla, P. A. Weiss, L. E. *J. Biomed. Mater. Res.* **1999**, *47*, 324–335.
[24] Williams, J. M. Adewunmi, A. Schek, R. M. Flanagan, C. L. Krebsbach, P. H. Feinberg, S. E. Hollister, S. J. Das, S. *Biomaterials* **2005**, *26*, 4817–4827.
[25] Xiong, Z. Yan, Y. Wang, S. Zhang, R. Zhang, C. *Scr. Mater.* **2002**, *46*, 771–776.
[26] Sun, W. Darling, A. Starly, B. Nam, J. *J. Biotech. Appl. Biochem.* **2004**, *39*, 29–47.
[27] Sun, W. Starly, B. Darling, A. Gomez, C. *J. Biotech. Appl. Biochem.* **2004**, *39*, 49–58.
[28] Wang, T. Feng, Z. *Mater. Lett.* **2005**, *59*, 2277–2280.
[29] Toyras, J. Nieminen, M. T. Kroger, H. Jurvelin, J. S. *Bone* **2002**, *31*, 503–507.

